RESEARCH ARTICLE

ADVANCED MATERIALS
www.advmat.de

Vertical-Structure Overcomes the Strain Limit of Stretchable Organic Electrochemical Transistors

Shilei Dai, Xinran Zhang, Xu Liu, Xinyu Tian, Binbin Cui, Ivo Pang, Haixuan Luo, Dingyao Liu, Xuecheng He, Xiaonan Chen, Junyao Zhang, Zhongrui Wang, Jia Huang, and Shiming Zhang**

Intrinsically stretchable organic electrochemical transistors (IS-OECTs), utilizing organic mixed ionic-electronic conductors (OMIECs) as their channel materials, have drawn great attention recently because of their potential to enable seamless integration between bioelectronic devices and living systems. However, the fabrication of IS-OECTs presents challenges due to the limited availability of OMIEC materials that possess the desired combination of mechanical and electrical properties. In this work, 1) we report the first successful fabrication of a vertical intrinsically stretchable OECT (VIS-OECT), achieved by using elastoadhesive electrodes; 2) we experimentally proved that vertical architecture can push the strain limit of an IS-OECT from 20% to 50%; and 3) the above finding introduces an unconventional design concept: the strain limit of an IS-OECT can surpass the intrinsic stretchability of the constituent OMIECs by employing vertical structure.

1. Introduction

Organic electrochemical transistors (OECTs) have garnered significant attention due to their ability to convert ionic signals to electronic signals within an organic mixed ionic-electronic conductor (OMIEC) channel.[1–4] These transistors benefit from OMIECs' unique properties, such as efficient ion-electron coupling and high volumetric capacitance, leading to low-voltage operation (<1 V), high transconductance (G_m),[5–8] and allowing signal amplification on-site.[9,10] These distinctive characteristics make OECTs a competitive technology for various applications such as biosensors[11–17] and neuromorphic computing.[18–24]

To fully unlock the potential of OECTs for skin-interfaced biosensing and biocomputing applications, achieving tissue-like stretchability is paramount.[25–30] This ensures a seamless OECT-tissue interface, reducing mechanical-incompatibility, alleviating wearing discomfort, and ultimately facilitating high-fidelity signal detection, transduction, and processing.[29–32]

So far, the fabrication of stretchable OECTs (S-OECTs) poses notable hurdles because there is a scarcity of OMIECs with the requisite blend of mechanical and electrical properties. Poly(3,4-ethylenedioxythiophene) polystyrene sulfonate (PEDOT: PSS), widely recognized as the "silicon material" for OECTs, owns an intrinsical stretchability of less than 5% when processed into thin films.[33,34] To tackle this challenge, extensive research has been conducted.[35–37] Zhang et al., demonstrated the first S-OECTs using a pre-stretched polydimethylsiloxane (PDMS) substrate. The device showed a modest G_m of 0.6 mS (channel width normalized G_m (i.e., $G_{m,\,w}$) of 0.3 mS mm^{-1}) at 30% strain.[35] Marchiori et al. introduced laser-patterned metallic interconnections featuring serpentine structures for S-OECTs, showcasing peak drain currents of 2.8 mA in the unstretched state and 0.2 mA under a 38% strain.[36] More recently, porous semiconductors with biaxially pre-stretched substrates have also been employed to realize S-OECTs, demonstrating a G_m of 3 mS ($G_{m,\,w}$ = 120 mS mm^{-1}) within 10^4 stretching cycles.[37]

Intrinsically stretchable OECTs (IS-OECTs), featured with high mechanical robustness, were developed in 2019 by precisely controlling the thickness and morphology of both the PEDOT: PSS channel and electrodes on an elastic substrate.[26] The resulting IS-OECT maintains consistent electrical performance within a 30% strain range, with a maximum G_m of 200 µS ($G_{m,\,w}$ = 0.1 mS mm^{-1}). Given the limited intrinsic stretchability of PEDOT: PSS thin films, material engineering (e.g., blending with surfactants) is introduced, which may sacrifice the material's electrical performance.[38] In more recent developments, Liu et al. significantly improved the performance of PEDOT: PSS IS-OECTs by using low-oxygen permeable elastomers as substrates.[39]

Despite the aforementioned progress, the field of S-OECTs, particularly IS-OECTs, remains in its infancy, requiring further studies for continued advancement. Among many challenges,

---

S. Dai, X. Zhang, X. Tian, B. Cui, I. Pang, H. Luo, D. Liu, X. He, X. Chen, Z. Wang, S. Zhang
Department of Electrical and Electronic Engineering
The University of Hong Kong
Hong Kong SAR 999077, P. R. China
E-mail: szhang@eee.hku.hk

X. Liu, J. Zhang, J. Huang
School of Materials Science and Engineering
Tongji University
Shanghai201804, P. R. China
E-mail: huangjia@tongji.edu.cn

The ORCID identification number(s) for the author(s) of this article can be found under https://doi.org/10.1002/adma.202413951

DOI: 10.1002/adma.202413951

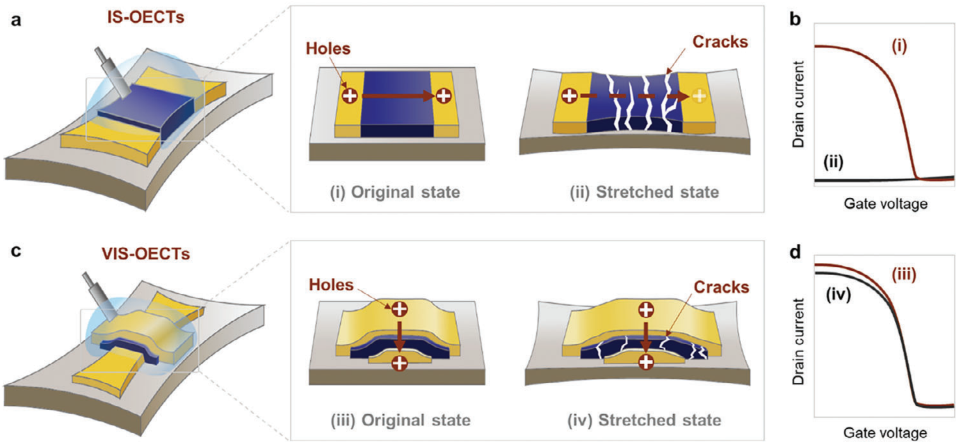

Figure 1. Comparison between VIS-OECTs and IS-OECTs. a) Schematics of the IS-OECTs and their 2D conductive pathways in (i) the original state and (ii) the stretched state. b) The schematic shows the transfer curves of the IS-OECTs. c) Schematics of the VIS-OECTs and their 3D conductive pathways in (iii) the original state and (iv) the stretched state. d) The schematic shows the transfer curves of the VIS-OECTs.

a key one lies in how to improve the intrinsic stretchability of IS-OECTs without compromising the electrical properties of the channel material.

Here, we report vertical IS-OECTs (VIS-OECTs), offering a solution to simultaneously enhance stretchability and G_m of OECTs through structural design, without compromising the other properties of the channel (**Figure 1**). Different from traditional structure design such as buckling or wavy methods, our approach incorporates 3D structural design into an intrinsically stretchable device. The channel is vertically stacked between the source and drain (S/D) electrodes, contrasting with traditional planar IS-OECTs. The resultant VIS-OECTs showed enhanced stretchability up to 50% strain without compromising electrical performance. In contrast, the planar-structured devices can only withstand a strain of less than 20%. Moreover, the VIS-OECTs outperform previously reported IS-OECTs in terms of G_m, showing over 100 times improvement (≈20 vs ≈0.2 mS). The simultaneous enhancements in both strain limit and G_m make VIS-OECTs a new device paradigm for broad tissue-interfaced bioelectronic applications.

2. Results and Discussion

2.1. Design of the VIS-OECTs

The limited stretchability of OMIECs, e.g., PEDOT: PSS, when forming planar-structure IS-OECTs, often results in device failure due to the formation of significant cracks perpendicular to the stretching direction within the OMIEC film (Figure 1a,b). These cracks disrupt the planar conductive pathway between the S/D electrodes. Since the cracks only stop current flow in the 2D plane, not 3D, we thus hypothesize that positioning the channel 3D, vertically between S/D electrodes, should mitigate the effect of strain on the device performance (Figure 1c,d).

To fabricate VIS-OECTs, challenges were encountered. First, the S/D electrodes used in VIS-OECTs should possess a blend of chemical inertness, high stretchability, and conductivity. Second, the preparation process for these stretchable electrodes should be easily achievable and compatible with the manufacturing processes of the 3D vertical structure. Third, the formation process of the 3D vertical structure should be compatible with the organic and elastic substrates. We tackled the electrode challenges by thermal evaporating of gold (Au) on the styrene-ethylene-butylene-styrene (SEBS) thermoplastic elastomer, creating an interpenetrating layer within the surface of the self-adhesive SEBS. Consequently, the VIS-OECTs are established by transferring the Au-SEBS strip electrode onto the top of the OMIEC film, resulting in a sandwich structure of SEBS-Au/OMIEC/Au-SEBS. The transfer process is compatible with the elastic substrate and easily forms the 3D vertical channel structure without requiring complicated manufacturing processes.

2.2. Fabrication of the VIS-OECTs

The process flow to fabricate VIS-OECT is shown in **Figure 2a**. The fabrication begins with the deposition of stretchable microcrack-Au electrodes on a SEBS substrate. During thermal evaporation of Au, the SEBS substrate was heated to 85–95 °C, significantly surpassing the glass transition temperature (T_g) of the hard polystyrene segments (T_g = 50–70 °C) of SEBS, making the electrodes elastoadhesive[40] Consequently, SEBS was sufficiently softened, producing highly mobile polymer chains, thus enabling Au atoms to penetrate into SEBS and form a biphasic interface with SEBS.[41] We conducted a thorough investigation into the stretchability of the microcrack-Au electrode, as depicted in Figure S1 (Supporting Information). The results showed that the microcrack-Au can be stretched to 100% strain while still maintaining an excellent conductivity (Figure S1a, Supporting Information). Moreover, the electrode can endure 100% strain over 100 cycles without major deterioration in conductivity (Figure S1b, Supporting Information). The remarkable stretchability and conductivity of the microcrack-Au electrode can be attributed to the formation of an interpenetrating layer with SEBS.[41] This layer plays a pivotal role in mitigating extensive crack formation, as illustrated by optical images (Figure S2, Supporting Information). We further studied the chemical stability of evaporated Au on the SEBS substrate

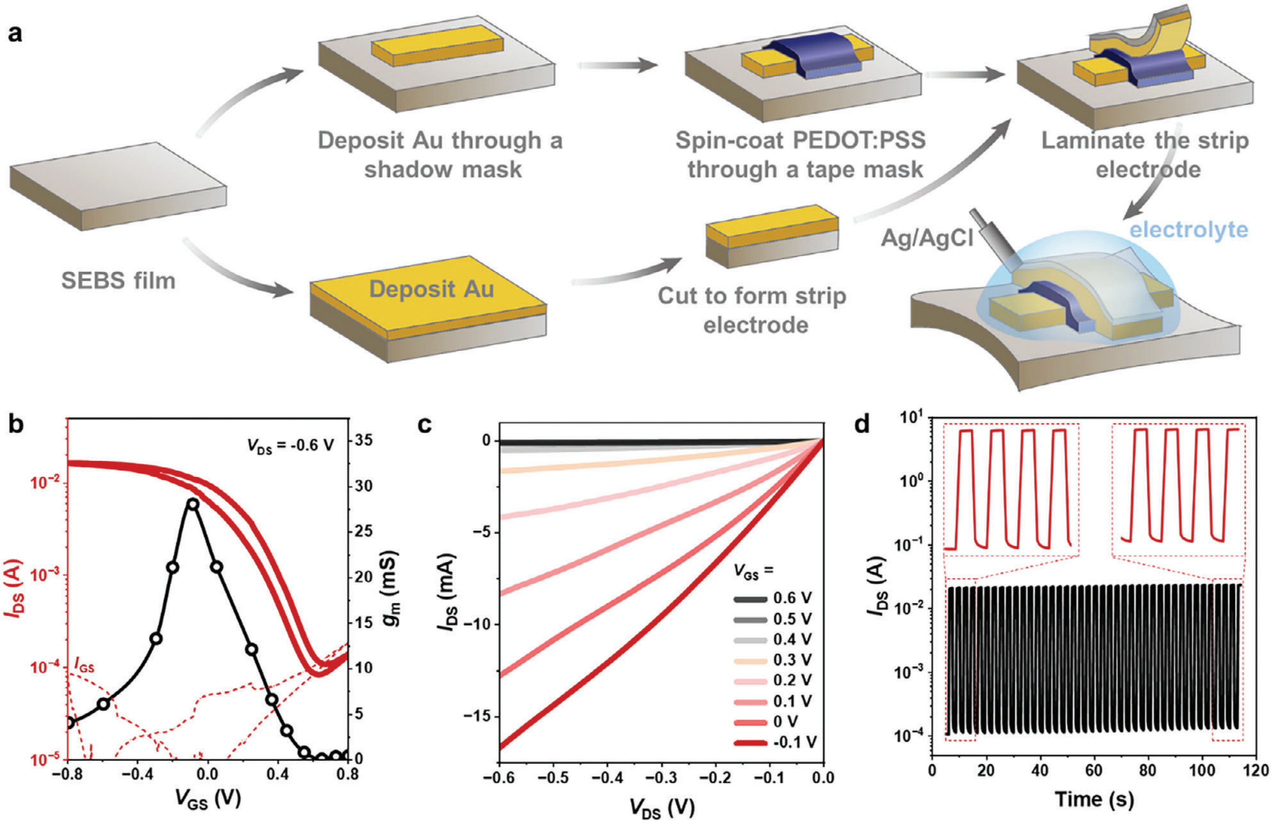

Figure 2. Fabrication and characterization of the VIS-OECTs. a) Fabrication process flow of the VIS-OECTs. b) The transfer curves, c) the output curves, and d) the transient responses of the VIS-OECTs. The cyclic transient behavior of the VIS-OECTs was measured by pulsing the V_{GS} from 0.6 to −0.4 V for 50 cycles at a fixed V_{DS} of −0.6 V.

using cyclic voltammetry (*CV*). As depicted in Figure S3 (Supporting Information), the microcrack-Au on the SEBS substrate exhibited comparable electrochemical performance to that of conventional Au electrode. Next, the PEDOT: PSS channel was formed by spin-coating formulated PEDOT: PSS suspension on microcrack-Au, followed by annealing at 120 °C for 40 min. Assembling of the VIS-OECT is finalized by transferring the microcrack-Au/SEBS strip electrode onto the PEDOT: PSS channel. To improve the adhesion between the top electrode and the bottom SEBS substrate, the assembled device was heated to 100 °C for 40 min. This annealing temperature significantly exceeds the T_g of the hard polystyrene segments of SEBS, thus improving adhesion between the elastoadhesive Au/SEBS electrode and the SEBS substrate due to increased chain mobility accompanied by volume expansion.[40] The interface bonding strength was investigated by using a typical 180° peeling test (Figure S4, Supporting Information). After annealing, the interfacial adhesion force between SEBS and Au/SEBS increased over an order of magnitude, thereby preventing delamination during device stretching (Figure S5 i, ii, Supporting Information).

2.3. Electrical performance of the VIS-OECTs

To evaluate the electrical performance of VIS-OECTs, 0.1 M NaCl solution was added to the 3D vertical channel as the electrolyte, with Ag/AgCl serving as the gate electrode, as illustrated in Figure S5 (iii) (Supporting Information). The VIS-OECTs exhibit typical depletion-mode operational characteristics (Figure 2b,c).[35,39] The device performance remained stable after cyclic transient measurements (Figure 2d). The transfer curve was measured by sweeping the gate voltage (V_{GS}) from 0.8 to −0.8 V in a voltage step of 5 mV at a constant drain voltage (V_{DS}) of −0.6 V. As shown in Figure 2c, the VIS-OECTs showed a maximum drain-current (I_{DS}) exceeding 16 mA, and an on/off ratio of $\approx 2 \times 10^2$. In the unstretched state, the G_m of VIS-OECT reached a value of 27 mS, which is 100 times higher than the referenced IS-OECTs (Table S1, Supporting Information). This is because OECTs' G_m is directly proportional to Wd/L.„ where W, d, and L stand for the channel width, thickness, and length, respectively.[42] The high G_m of VIS-OECTs stems from the small channel length,[43] which is defined by the thickness of PEDOT: PSS channel.

Figure S6a–c (Supporting Information) compares the transfer curves of different VIS-OECT devices. The similar transfer curves of these devices indicate a good reproducibility. To prove the versatility of our vertical structure design, we further employed a polythiophene-based OMIEC, named namely poly(2-(3,3′-bis(2-(2-(2-methoxyethoxy) ethoxy) ethoxy)-[2,2′-bithiophen]-5) yl thiophene) (p(g2T-T)), for the fabrication of enhancement-mode VIS-OECTs (see Experimental Section). As shown in Figure S6d–f (Supporting Information),

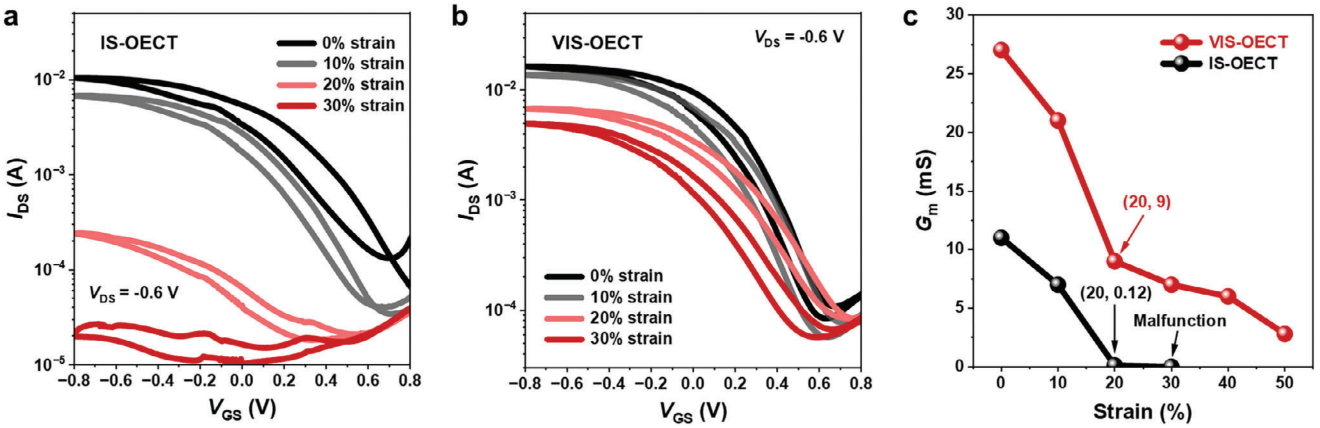

Figure 3. Performance comparison between VIS-OECTs and IS-OECTs. Transfer curves of a) IS-OECTs and b) VIS-OECTs under various stretching conditions. c) The G_m values of VIS-OECTs and IS-OECTs as a function of strain.

p(g2T-T)-based VIS-OECTs also demonstrated excellent performance. We observed that VIS-OECTs utilizing p(g2T-T) showed a lower off-current (≈2 µA) and leakage current in comparison to depletion-mode VIS-OECTs based on PEDOT: PSS (Figure S7, Supporting Information). This disparity can be ascribed to differences between their inherent conductivities.

2.4. Electromechanical Performance of the VIS-OECTs

In our subsequent investigation, we provide evidence demonstrating the exceptional ability of the 3D, vertical OECT structure to exceed the strain limits of OMIECs. For a fair comparison, both IS-OECTs and VIS-OECTs were fabricated using identical experimental materials and conditions, differing only in their device structure. Before assessing the devices' stretchability, we examined the optical images and relative resistance (R/R_0) of the PEDOT: PSS film used in device fabrication under various strain conditions, as shown in Figure S8 (Supporting Information). Here, R_0 represents the initial resistance, while R indicates the resistance under different strain levels. The R/R_0 ratio of the PEDOT: PSS film increases significantly—by several orders of magnitude—once the strain surpasses 30%, consistent with optical images that reveal a substantial number of cracks in the film at this strain level. To evaluate the device stretchability, IS-OECTs were stretched from 0% to 30% strain, while VIS-OECTs were stretched from 0% to 50% strain, both in 10% strain increments. **Figure** 3a,b depict the transfer curves of IS-OECTs and VIS-OECTs under various stretching conditions, respectively. It is evident that IS-OECTs function only at strains below 10% and fail completely at 30% strain (Figure 3a). The primary cause of functionality loss in IS-OECTs at 30% strain is because the strain-induced cracks that disrupt the conductive pathways within the planar structure. Incontrast, the VIS-OECTs, constructed using the same PEDOT: PSS film, maintained functional even at 50% strain (Figure S9, Supporting Information). This not only surpasses the stretchability of the planar-structured IS-OECTs but also exceeds the inherent stretchability of the PEDOT: PSS film (Figure S8, Supporting Information). It is worth noting that while lateral stretching can create vertical stress on the film, this stress can be alleviated when significant cracks perpendicular to the substrate appear. If cracks parallel to the substrate were induced by vertical stress, we would expect to observe interlayer slip in specific regions of the stretched film. However, the optical images in Figure S8 (Supporting Information) did not reveal any interlayer slip in the stretched film. These experimental results support our key hypothesis that positioning the channel 3D, vertically between the S/D electrodes can mitigate the impact of strain on OMIECs channel (Figure 1c,d).

The G_m values of both IS-OECTs and VIS-OECTs under various strain conditions are compared in Figure 3c. Although IS-OECTs still function at 20% strain, their G_m (@20% strain) is only 0.12 mS, which is 75 times lower than that of VIS-OECTs at 20% strain, and 23 times lower than VIS-OECTs at 50% strain. The decrease in G_m of VIS-OECT under strain can be partially attributed to the increase in electrode resistance at high strain levels (Figure S1a, Supporting Information), which results in a decrease in the effective V_{DS} during stretching. The deterioration of the interface with increasing stretching may be another reason.

2.5. VIS-OECTs for Wearable Computing

VIS-OECTs have the potential to assemble stretchable crossbars (**Figure** 4a).[44] The VIS-OECTs can serve as stretchable nodes of the crossbar for implementing various artificial neural networks. The vertical structure cases the manufacturing process and upscaling of device density.[45] As an example, we use VIS-OECTs as nodes for stretchable reservoir computing (RC),[46–52] relevant for wearable edge-intelligence and AI health.

Nonlinear response and fading memory are two pivotal characteristics of RC networks, signifying that the reservoir state is affected by input from the recent past while remaining independent of input from the distant past.[48] The potential of the VIS-OECTs as nodes for physical RC implementation was initially explored by testing their nonlinear response and fading memory effect under sequential gate pulses. As shown in Figure 4b, our VIS-OECTs exhibit a nonlinear dynamic response to sequence patterns and demonstrate clear fading memory characteristics

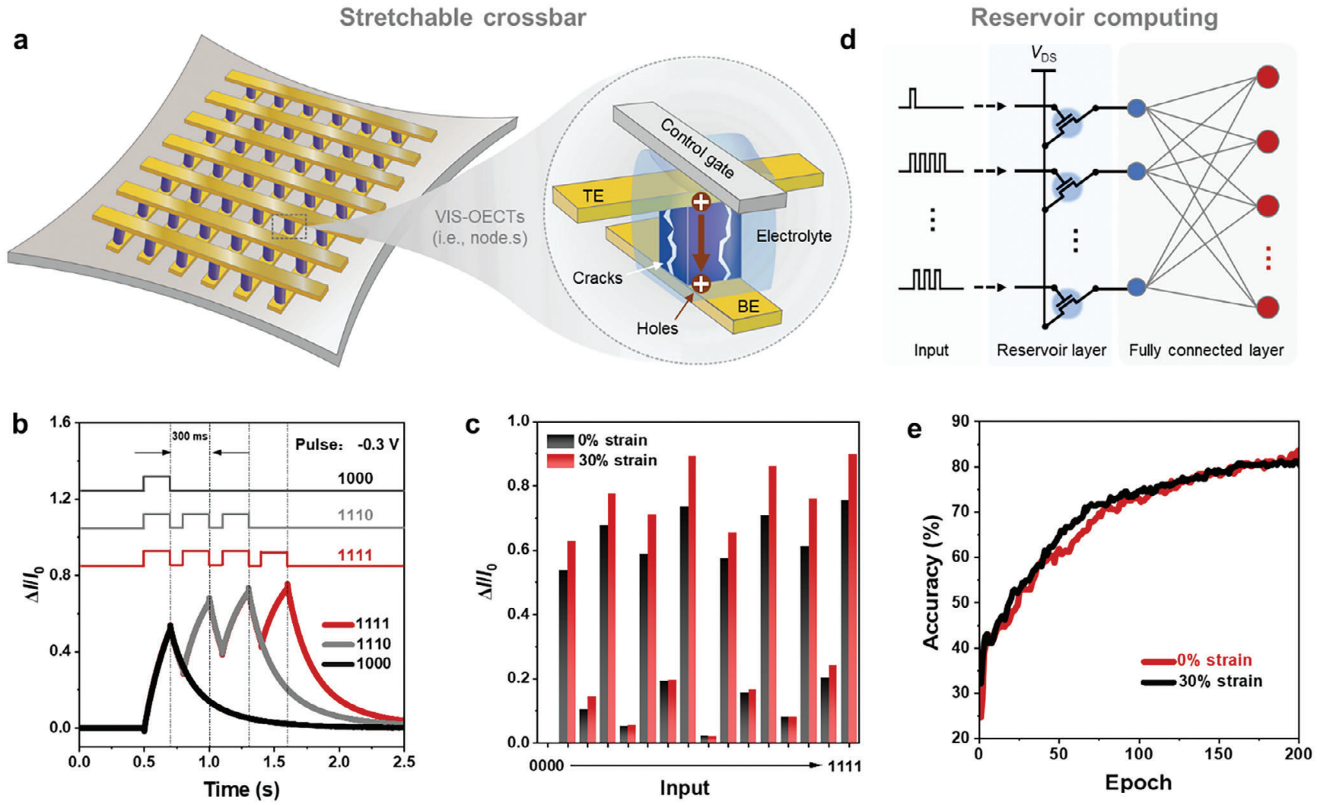

Figure 4. VIS-OECTs for stretchable neuromorphic computing. a) Schematic of the stretchable crossbar based on VIS-OECTs. b) Illustration of the nonlinear response and fading memory of VIS-OECT for different sequential inputs. ΔI represents the change in drain current induced by the sequential gate pulses, while I_0 denotes the initial drain current in the absence of gate pulses. The current is measured at a V_{DS} of −0.6 V. c) Reservoir states of VIS-OECTs are used to differentiate between different temporal inputs at 0% strain and 30% strain, respectively. d) Schematic diagram illustrating reservoir computing implemented with the VIS-OECTs array as the reservoir layer. e) Classification accuracy for different hand gestures as a function of the training epoch.

when spikes end. To further assess the performance of the VIS-OECTs as nodes for physical RC implementation, we used them to differentiate16 pulse sequence patterns ranging from 0000 to 1111, as illustrated in Figure 4c. In this context, "0" signifies that no pulse is applied to the gate terminal, while "1" indicates the application of a pulse of −0.3 V, 200 ms. The VIS-OECTs-based RC nodes can effectively distinguish 16 different pulse patterns at the end of the pulse sequence (Figure 4c), demonstrating its potential application in temporal information processing. More significantly, the VIS-OECTs are capable of differentiating patterns after being stretched to 30% strain, surpassing the strain limits of PEDOT: PSS thin films (Figure S10, Supporting Information).

To showcase the potential of our VIS-OECTs for wearable edge-computing applications, we present their application in hand gesture recognition utilizing recorded electromyography (EMG) signals. The EMG signal was initially captured by an EMG sensor as described in our recent work.[53] Then, we employed a sliding window (with a size of 640 ms and a stride of 40 ms) to segment the temporal EMG signals and convert them into sequential pulse streams. As shown in Figure 4d, the pulse streams are applied to the gate terminal of VIS-OECTs in the physical reservoir layer and then the corresponding source-drain currents are sent to the software-based fully connected neural network for classification. As depicted in Figure 4e, after training for 200 epochs, the classification accuracy for different hand gestures exceeded 80%. There was no significant decrease in accuracy at 30% strain, indicating the robustness of our VIS-OECTs which facilitates their deployment in wearable scenarios.

3. Conclusion

In this work, we report the first fabrication of VIS-OECTs. Unlike planar-structure IS-OECTs, the proposed VIS-OECTs feature a 3D, vertical, and strain-insensitive conductive path. As a result, the stretchability of the VIS-OECT surpassed the strain limit of the constituent semiconductor. It is worth mentioning that, unlike structure-endowed stretchability in non-intrinsically stretchable devices, the vertical structure improves the stretchability of intrinsically stretchable devices without compromising their potential for further integration.

Previous research has demonstrated vertical OECTs,[54–56] showcasing their potential in diverse applications such as bio-signal sensing and amplification,[57–59] complementary circuits,[45,60–62] and neuromorphic computing.[63–66] However, these studies have not explored the use of vertical OECTs to address the challenges of device mechanics.

The following issues are observed during the development of VIS-OECT which can be further investigated. First, compared to planar OECTs, VIS-OECTs need elastoadhesive electrodes with stable electrochemical properties, making it essential to develop strain-insensitive, adhesive, and inert electrodes that can be easily patterned at scale.[67] Second, precise control of the adhesion between all functional layers is essential. Surface functionalization can be further explored such as interface crosslinking[68]; Third, the fabrication of VIS-OECTs at scale has not yet been achieved, where advanced manufacturing technologies, such as transfer printing, could potentially be utilized.[69–72] Finally, tissue-like functions such as gas permeability and biocompatibility can be further explored to promote their interfacing with living systems.[73–76]

4. Experimental Section

Materials: Poly(3,4-ethylenedioxythiophene): poly (styrene sulfonate) (PEDOT: PSS) aqueous solution (Clevios PH1000) was purchased from Heraeus Deutschland GmbH & Co. KG. 4-Dodecylbenzenesulfonic acid (DBSA), sodium chloride, (3-glycidyloxypropyl) trimethoxysilane (GOPS) and ethylene glycol (EG) were purchased from Sigma–Aldrich and used as received. Styrene-ethylene-butylene-styrene (SEBS H1062) was provided by Asahi Kasei. Poly(2-(3,3′-bis(2-(2-(2-methoxyethoxy) ethoxy) ethoxy)-[2,2′-bithiophen]-5) yl thiophene) (p(g2T-T)) was synthesized according to the literature report.[27] The azide-based crosslinker 2,2-bis(((4-azido2,3,5,6-tetrafluoroben-zoyl)-oxy) methyl) propane1,3-diylbis (4-azido-2,3,5,6 tetrafluoro benzoate) (4Bx) was synthesized following a procedure reported in the literature.[77]

Fabrication of PEDOT:PSS-Based VIS-OECTs: The fabrication of VIS-OECT began with the thermal evaporation of a 60–80 nm thick Au electrode onto the SEBS substrate, utilizing a shadow mask for precise patterning. During the deposition of Au, the supporting substrate within the chamber was heated to ≈90 °C. The evaporation rate of Au was maintained between 0.1 and 0.4 Å s^{-1}. The PEDOT: PSS solution was prepared by combining PH1000 with DBSA (0.5 v/v.%), GOPS (3 w/w.%), and EG (5 v/v.%). Subsequently, the mixed solution was filtered using a hydrophilic syringe filter with an aperture size of 0.45 µm to remove any aggregates, ensuring their suitability for further use. The obtained solution was spin-coated on the plasma-treated Au-SEBS substrate at 1000 rpm for 1 min with adhesive tape as the mask. After that, the mask was removed and the sample was annealed at 120 °C for 40 min. Then, a strip-shaped (1 mm wide) Au/SEBS electrode was directly laminated onto the PEDOT:PSS film, forming a SEBS-Au/PEDOT:PSS/Au-SEBS sandwich structure. The alignment was guided by utilizing the marks on the substrate. To enhance the adhesion force between each layer, the device was heated at 100 °C for 40 min.

Fabrication of PEDOT:PSS-Based IS-OECTs: The planar structured IS-OECTs were fabricated by directly spin-coating the PEDOT: PSS solution (i.e., same as the above processing procedures) on the Au-SEBS substrate (channel length 5 mm, channel width 1 mm). After that, the sample was annealed at 120 °C for 40 min.

Fabrication of p(g2T-T)-Based VIS-OECTs: The p(g2T-T) and 4Bx were dissolved in chloroform at a concentration of 5 and 2.8 mg mL^{-1}, respectively. The p(g2T-T) solution was stirred at 60 °C for more than 8 h before use. The p(g2T-T) solution was blended with 4Bx solution with a volume ratio of 8 to1. A 10–15 wt.% dextran solution in water was spin-coated onto a plasma-treated silicon wafer at 1500 rpm for 30 s. Subsequently, the wafer underwent baking on a hot plate first at 80 °C for 1 min followed by 180 °C for 30 min. The p(g2T-T) and 4Bx blended solution were spin-coated onto the dextran-coated wafer at 600 rpm for 1 min. Subsequently, the coated layer was cross-linked under 365 nm UV irradiation for 5 min using a mask aligner (URE-2000/35). To transfer the p(g2T-T) film, a PDMS film was laminated on top of the p(g2T-T) film. Subsequently, the sample was immersed in DI water to dissolve the underlying dextran layer. The p(g2T-T) film could be patterned by a blade after being transferred to PDMS. Before transferring the patterned p(g2T-T) film onto the Au-SEBS substrate, the Au-SEBS was exposed to UV ozone treatment for 3 min. Subsequently, the p(g2T-T) film was transferred from the PDMS to the Au-SEBS by carefully pressing the p(g2T-T) film onto the substrate and then gently removing the PDMS. Following this, a strip-shaped (1 mm wide) Au-SEBS electrode was laminated onto the p(g2T-T), forming SEBS-Au/p(g2T-T)/Au-SEBS sandwich structure. To enhance the adhesion force between each layer, the device was heated at 100 °C for 40 min.

RC Simulation: The process started with capturing EMG signals using EMG sensors, followed by segmenting these signals into sequential pulse streams using a sliding window technique (with a size of 640 ms and a stride of 40 ms) based on the previous work.[53] These pulse streams were then applied to the gate of the VIS-OECTs-based physical reservoir to measure the corresponding source-drain current. In the RC simulation workflow, pseudo-input data from 16 VIS-OECTs in the RC network were generated using the collected source-drain current. This data was then fed into the fully connected layer for processing, and accuracies were calculated as a result. To train the fully connected layer, the Adam optimizer was employed with a learning rate set at 0.01 and utilized the gradient descent method.

Characterization and Measurement: All device performances were assessed through testing in atmospheric conditions using a semiconductor characterization system (PDA-Fs Pro). A 0.1 M NaCl aqueous solution served as the electrolyte for all OECT testing. During testing, an Ag/AgCl pellet was immersed in the electrolyte as a gate electrode. Optical images were captured using an optical microscope. Cyclic voltammetry (*CV*) measurements were conducted using an electrochemical workstation.

Supporting Information

Supporting Information is available from the Wiley Online Library or from the author.

Acknowledgements

S.D., X.Z., and X.L. contributed equally to this work. S.Z. conceived this project, acquired funding and supervised the whole research. S.Z. acknowledges the Collaborative Research Fund (C7005-23Y) and Germany/Hong Kong Joint Research Scheme (G-HKU707/22) from the Research Grants Council (RGC) of the Hong Kong SAR Government and the Seed Funding for Strategic Interdisciplinary Research Scheme (SIRS) from the University of Hong Kong. S.D. acknowledges the RGC Postdoctoral Fellowship Scheme (PDF2324-7S07).

Conflict of Interest

The authors declare no conflict of interest.

Data Availability Statement

The data that support the findings of this study are available from the corresponding author upon reasonable request.

Keywords

stretchable OECTs, vertical structure, PEDOT: PSS, biosensing, biocomputing

Received: September 16, 2024
Revised: November 13, 2024

[1] S. T. Keene, J. E. M. Laulainen, R. Pandya, M. Moser, C. Schnedermann, P. A. Midgley, I. McCulloch, A. Rao, G. G. Malliaras, *Nat. Mater.* **2023**, *22*, 1121.
[2] E. Zeglio, O. Inganäs, *Adv. Mater.* **2018**, *30*, 1800941.
[3] H. Sun, J. Gerasimov, M. Berggren, S. Fabiano, *J Mater. Chem. C* **2018**, *6*, 11778.
[4] P. Romele, M. Ghittorelli, Z. M. Kovács-Vajna, F. Torricelli, *Nat. Commun.* **2019**, *10*, 3044.
[5] J. Rivnay, S. Inal, A. Salleo, R. M. Owens, M. Berggren, G. G. Malliaras, *Nat. Rev. Mater.* **2018**, *3*, 17086.
[6] F. Torricelli, D. Z. Adrahtas, Z. Bao, M. Berggren, F. Biscarini, A. Bonfiglio, C. A. Bortolotti, C. D. Frisbie, E. Macchia, G. G. Malliaras, I. McCulloch, M. Moser, T. Q. Nguyen, R. M. Owens, A. Salleo, A. Spanu, L. Torsi, *Nat. Rev. Methods Primers* **2021**, *1*, 66.
[7] L. Xiang, L. Liu, F. Zhang, C.-a. Di, D. Zhu, *Adv. Funct. Mater.* **2021**, *31*, 2102149.
[8] D. Ohayon, V. Druet, S. Inal, *Chem. Soc. Rev.* **2023**, *52*, 1001.
[9] O. Parlak, S. T. Keene, A. Marais, V. F. Curto, A. Salleo, *Sci. Adv.* **2018**, *4*, eaar2904.
[10] C. Cea, Z. Zhao, D. J. Wisniewski, G. D. Spyropoulos, A. Polyravas, J. N. Gelinas, D. Khodagholy, *Nat. Mater.* **2023**, *22*, 1227.
[11] A. Nawaz, Q. Liu, W. L. Leong, K. E. Fairfull-Smith, P. Sonar, *Adv. Mater.* **2021**, *33*, 2101874.
[12] Y. Li, B. Cui, S. Zhang, B. Li, J. Li, S. Liu, Q. Zhao, *Small* **2022**, *18*, 2107413.
[13] H. Liu, A. Yang, J. Song, N. Wang, P. Lam, Y. Li, H. K. Law, F. Yan, *Sci. Adv.* **2021**, *7*, eabg8387.
[14] Y. Yao, W. Huang, J. Chen, X. Liu, L. Bai, W. Chen, Y. Cheng, J. Ping, T. J. Marks, A. Facchetti, *Adv. Mater.* **2023**, *35*, 2209906.
[15] K. Guo, S. Wustoni, A. Koklu, E. Díaz-Galicia, M. Moser, A. Hama, A. A. Alqahtani, A. N. Ahmad, F. S. Alhamlan, M. Shuaib, A. Pain, I. McCulloch, S. T. Arold, R. Grünberg, S. Inal, *Nat. Biomed. Eng.* **2021**, *5*, 666.
[16] G. Frusconi, Z. M. Kovács-Vajna, F. Torricelli, *Adv. Mater. Technol.* **2024**, *9*, 2400301.
[17] K. Lieberth, A. Pavlou, D. Harig, P. W. M. Blom, P. Gkoupidenis, F. Torricelli, *Adv. Mater. Technol.* **2023**, *8*, 2201697.
[18] E. R. W. van Doremaele, X. Ji, J. Rivnay, Y. van de Burgt, *Nat. Electron.* **2023**, *6*, 765.
[19] Y. Zhang, E. R. W. van Doremaele, G. Ye, T. Stevens, J. Song, R. C. Chiechi, Y. van de Burgt, *Adv. Mater.* **2022**, *34*, 2200393.
[20] E. R. W. van Doremaele, P. Gkoupidenis, Y. van de Burgt, *J. Mater. Chem. C* **2019**, *7*, 12754.
[21] S. T. Keene, C. Lubrano, S. Kazemzadeh, A. Melianas, Y. Tuchman, G. Polino, P. Scognamiglio, L. Cinà, A. Salleo, Y. van de Burgt, F. Santoro, *Nat. Mater.* **2020**, *19*, 969.
[22] T. Sarkar, K. Lieberth, A. Pavlou, T. Frank, V. Mailaender, I. McCulloch, P. W. M. Blom, F. Torricelli, P. Gkoupidenis, *Nat. Electron.* **2022**, *5*, 774.
[23] P. C. Harikesh, C. Y. Yang, H. Y. Wu, S. Zhang, M. J. Donahue, A. S. Caravaca, J. D. Huang, P. S. Olofsson, M. Berggren, D. Tu, S. Fabiano, *Nat. Mater.* **2023**, *22*, 242.
[24] P. Belleri, J. Pons i Tarrés, I. McCulloch, P. W. M. Blom, Z. M. Kovács-Vajna, P. Gkoupidenis, F. Torricelli, *Nat. Commun.* **2024**, *15*, 5350.
[25] Y. Li, N. Wang, A. Yang, H. Ling, F. Yan, *Adv. Electron. Mater.* **2019**, *5*, 1900566.
[26] S. Zhang, Y. Li, G. Tomasello, M. Anthonisen, X. Li, M. Mazzeo, A. Genco, P. Grutter, F. Cicoira, *Adv. Electron. Mater.* **2019**, *5*, 1900191.
[27] Y. Dai, S. Dai, N. Li, Y. Li, M. Moser, J. Strzalka, A. Prominski, Y. Liu, Q. Zhang, S. Li, H. Hu, W. Liu, S. Chatterji, P. Cheng, B. Tian, I. McCulloch, J. Xu, S. Wang, *Adv. Mater.* **2022**, *34*, 2201178.
[28] H. Lee, S. Lee, W. Lee, T. Yokota, K. Fukuda, T. Someya, *Adv. Funct. Mater.* **2019**, *29*, 1906982.
[29] S. Dai, Y. Dai, Z. Zhao, F. Xia, Y. Li, Y. Liu, P. Cheng, J. Strzalka, S. Li, N. Li, Q. Su, S. Wai, W. Liu, C. Zhang, R. Zhao, J. J. Yang, R. Stevens, J. Xu, J. Huang, S. Wang, *Matter* **2022**, *5*, 3375.
[30] W. Lee, S. Kobayashi, M. Nagase, Y. Jimbo, I. Saito, Y. Inoue, T. Yambe, M. Sekino, G. G. Malliaras, T. Yokota, M. Tanaka, T. Someya, *Sci. Adv.* **2018**, *4*, eaau2426.
[31] N. Li, Y. Li, Z. Cheng, Y. Liu, Y. Dai, S. Kang, S. Li, N. Shan, S. Wai, A. Ziaja, Y. Wang, J. Strzalka, W. Liu, C. Zhang, X. Gu, J. A. Hubbell, B. Tian, S. Wang, *Science* **2023**, *381*, 686.
[32] W. Wang, Z. Li, M. Li, L. Fang, F. Chen, S. Han, L. Lan, J. Chen, Q. Chen, H. Wang, C. Liu, Y. Yang, W. Yue, Z. Xie, *Nano-Micro Lett.* **2022**, *14*, 184.
[33] D. Won, J. Kim, J. Choi, H. Kim, S. Han, I. Ha, J. Bang, K. K. Kim, Y. Lee, T. S. Kim, J. H. Park, C. Y. Kim, S. H. Ko, *Sci. Adv.* **2022**, *8*, eabo3209.
[34] N. Matsuhisa, X. Chen, Z. Bao, T. Someya, *Chem. Soc. Rev.* **2019**, *48*, 2946.
[35] S. Zhang, E. Hubis, G. Tomasello, G. Soliveri, P. Kumar, F. Cicoira, *Chem. Mater.* **2017**, *29*, 3126.
[36] B. Marchiori, R. Delattre, S. Hannah, S. Blayac, M. Ramuz, *Sci. Rep.* **2018**, *8*, 8477.
[37] J. Chen, W. Huang, D. Zheng, Z. Xie, X. Zhuang, D. Zhao, Y. Chen, N. Su, H. Chen, R. M. Pankow, Z. Gao, J. Yu, X. Guo, Y. Cheng, J. Strzalka, X. Yu, T. J. Marks, A. Facchetti, *Nat. Mater.* **2022**, *21*, 564.
[38] Y. Li, S. Zhang, X. Li, V. R. N. Unnava, F. Cicoira, *Flex. Print. Electron* **2019**, *4*, 044004.
[39] D. Liu, X. Tian, J. Bai, Y. Wang, Y. Cheng, W. Ning, P. K. L. Chan, K. Wu, J. Sun, S. Zhang, *Adv. Sci.* **2022**, *9*, 2203418.
[40] R. J. Angelo, R. M. Ikeda, M. L. Wallach, *Polymer* **1965**, *6*, 141.
[41] Y. Jiang, S. Ji, J. Sun, J. Huang, Y. Li, G. Zou, T. Salim, C. Wang, W. Li, H. Jin, J. Xu, S. Wang, T. Lei, X. Yan, W. Y. X. Peh, S. C. Yen, Z. Liu, M. Yu, H. Zhao, Z. Lu, G. Li, H. Gao, Z. Liu, Z. Bao, X. Chen, *Nature* **2023**, *614*, 456.
[42] J. Rivnay, P. Leleux, M. Ferro, M. Sessolo, A. Williamson, D. A. Koutsouras, D. Khodagholy, M. Ramuz, X. Strakosas, R. M. Owens, C. Benar, J. M. Badier, C. Bernard, G. G. Malliaras, *Sci. Adv.* **2015**, *1*, e1400251.
[43] M. J. Donahue, A. Williamson, X. Strakosas, J. T. Friedlein, R. R. McLeod, H. Gleskova, G. G. Malliaras, *Adv. Mater.* **2018**, *30*, 1705031.
[44] Y. Choi, S. Oh, C. Qian, J. H. Park, J. H. Cho, *Nat. Commun.* **2020**, *11*, 4595.
[45] J. Kim, R. M. Pankow, Y. Cho, I. D. Duplessis, F. Qin, D. Meli, R. Daso, D. Zheng, W. Huang, J. Rivnay, T. J. Marks, A. Facchetti, *Nat. Electron.* **2024**, *7*, 234.
[46] R. Chen, H. Yang, R. Li, G. Yu, Y. Zhang, J. Dong, D. Han, Z. Zhou, P. Huang, L. Liu, X. Liu, J. Kang, *Sci. Adv.* **2024**, *10*, eadl1299.
[47] X. Liang, J. Tang, Y. Zhong, B. Gao, H. Qian, H. Wu, *Nat. Electron.* **2024**, *7*, 193.
[48] L. Appeltant, M. C. Soriano, G. Van der Sande, J. Danckaert, S. Massar, J. Dambre, B. Schrauwen, C. R. Mirasso, I. Fischer, *Nat. Commun.* **2011**, *2*, 468.
[49] D. J. Gauthier, E. Bollt, A. Griffith, W. A. S. Barbosa, *Nat. Commun.* **2021**, *12*, 5564.
[50] S. Pecqueur, M. Mastropasqua Talamo, D. Guérin, P. Blanchard, J. Roncali, D. Vuillaume, F. Alibart, *Adv. Electron. Mater.* **2018**, *4*, 1800166.
[51] L. Petrauskas, M. Cucchi, C. Grüner, F. Ellinger, K. Leo, C. Matthus, H. Kleemann, *Adv. Electron. Mater.* **2022**, *8*, 2100330.
[52] C. Matteo, G. Christopher, P. Lautaro, S. Peter, T. Hsin, F. Axel, P. Bogdan, M. Christian, B. Peter, K. Hans, L. Karl, *Sci. Adv.* **2021**, *7*, eabh0693.
[53] D. Liu, X. Tian, J. Bai, S. Wang, S. Dai, Y. Wang, Z. Wang, S. Zhang, *Nat. Electron.* **2024**, https://doi.org/10.1038/s41928-024-01250-9.
[54] J. Brodský, I. Gablech, L. Migliaccio, M. Havlíček, M. J. Donahue, E. D. Głowacki, *ACS Appl. Mater. Interfaces* **2023**, *15*, 27002.

[55] J. Lenz, F. del Giudice, F. R. Geisenhof, F. Winterer, R. T. Weitz, *Nat. Nanotechnol.* **2019**, *14*, 579.
[56] C. Eckel, J. Lenz, A. Melianas, A. Salleo, R. T. Weitz, *Nano Lett.* **2022**, *22*, 973.
[57] I. Uguz, D. Ohayon, S. Yilmaz, S. Griggs, R. Sheelamanthula, J. D. Fabbri, I. McCulloch, S. Inal, K. L. Shepard, *Sci. Adv.* **2024**, *10*, eadi9710.
[58] R. B. Rashid, W. Du, S. Griggs, I. P. Maria, I. McCulloch, J. Rivnay, *Sci. Adv.* **2021**, *7*, eabh1055.
[59] M. Abarkan, A. Pirog, D. Mafilaza, G. Pathak, G. N'Kaoua, E. Puginier, R. O'Connor, M. Raoux, M. J. Donahue, S. Renaud, J. Lang, *Adv. Sci.* **2022**, *9*, 2105211.
[60] W. Huang, J. Chen, Y. Yao, D. Zheng, X. Ji, L. W. Feng, D. Moore, N. R. Glavin, M. Xie, Y. Chen, R. M. Pankow, A. Surendran, Z. Wang, Y. Xia, L. Bai, J. Rivnay, J. Ping, X. Guo, Y. Cheng, T. J. Marks, A. Facchetti, *Nature* **2023**, *613*, 496.
[61] D. U. Lim, S. B. Jo, J. H. Cho, *Adv. Mater.* **2023**, *35*, 2208757.
[62] Z. Deng, Y. Yu, Y. Zhou, J. Zhou, M. Xie, B. Tao, Y. Lai, J. Wen, Z. Fan, X. Liu, D. Zhao, L. W. Feng, Y. Cheng, C. G. Huang, W. Yue, W. Huang, *Adv. Mater.* **2024**, *36*, 2405115.
[63] S. Wang, X. Chen, C. Zhao, Y. Kong, B. Lin, Y. Wu, Z. Bi, Z. Xuan, T. Li, Y. Li, W. Zhang, E. Ma, Z. Wang, W. Ma, *Nat. Electron.* **2023**, *6*, 281.
[64] Y. Wang, A. Koklu, Y. Zhong, T. Chang, K. Guo, C. Zhao, T. C. H. Castillo, Z. Bu, C. Xiao, W. Yue, W. Ma, S. Inal, *Adv. Funct. Mater.* **2024**, *34*, 2304103.
[65] Z. Laswick, X. Wu, A. Surendran, Z. Zhou, X. Ji, G. M. Matrone, W. L. Leong, J. Rivnay, *Nat. Commun.* **2024**, *15*, 6309.
[66] Y. Choi, D. H. Ho, S. Kim, Y. J. Choi, D. G. Roe, I. C. Kwak, J. Min, H. Han, W. Gao, J. H. Cho, *Sci. Adv.* **2023**, *9*, eadg5946.
[67] D. Jung, C. Lim, H. J. Shim, Y. Kim, C. Park, J. Jung, S. I. Han, S. H. Sunwoo, K. W. Cho, G. D. Cha, D. C. Kim, J. H. Koo, J. H. Kim, T. Hyeon, D. H. Kim, *Science* **2021**, *373*, 1022.
[68] M. J. Kim, H. S. Ryu, Y. Y. Choi, D. H. Ho, Y. Lee, A. Tripathi, J. H. Son, Y. Lee, S. Kim, M. S. Kang, H. Y. Woo, J. H. Cho, *Sci. Adv.* **2021**, *7*, eabg8169.
[69] P. Andersson Ersman, R. Lassnig, J. Strandberg, D. Tu, V. Keshmiri, R. Forchheimer, S. Fabiano, G. Gustafsson, M. Berggren, *Nat. Commun.* **2019**, *10*, 5053.
[70] M. Massetti, S. Zhang, P. C. Harikesh, B. Burtscher, C. Diacci, D. T. Simon, X. Liu, M. Fahlman, D. Tu, M. Berggren, S. Fabiano, *npj Flex. Electron.* **2023**, *7*, 11.
[71] K. Sim, S. Chen, Z. Li, Z. Rao, J. Liu, Y. Lu, S. Jang, F. Ershad, J. Chen, J. Xiao, C. Yu, *Nat. Electron.* **2019**, *2*, 471.
[72] R. Granelli, I. Alessandri, P. Gkoupidenis, I. Vassalini, Z. M. Kovács-Vajna, P. W. M. Blom, F. Torricelli, *Small* **2022**, *18*, 2108077.
[73] B. Zhang, J. Li, J. Zhou, L. Chow, G. Zhao, Y. Huang, Z. Ma, Q. Zhang, Y. Yang, C. K. Yiu, J. Li, F. Chun, X. Huang, Y. Gao, P. Wu, S. Jia, H. Li, D. Li, Y. Liu, K. Yao, R. Shi, Z. Chen, B. L. Khoo, W. Yang, F. Wang, Z. Zheng, Z. Wang, X. Yu, *Nature* **2024**, *628*, 84.
[74] H. Sheng, J. Zhou, B. Li, Y. He, X. Zhang, J. Liang, J. Zhou, Q. Su, E. Xie, W. Lan, K. Wang, C. Yu, *Sci. Adv.* **2021**, *7*, eabe3097.
[75] E. W. C. Chan, X. Sun, Y. Uda, B. Zhu, D. Barker, J. Travas-Sejdic, *J. Mater. Chem. C* **2024**, *12*, 11157.
[76] C. Wang, C. Wang, Z. Huang, S. Xu, *Adv. Mater.* **2018**, *30*, 1801368.
[77] M. J. Kim, M. Lee, H. Min, S. Kim, J. Yang, H. Kweon, W. Lee, D. H. Kim, J. H. Choi, D. Y. Ryu, M. S. Kang, B. Kim, J. H. Cho, *Nat. Commun.* **2020**, *11*, 1520.